

# Spatial interactions and oscillatory tragedies of the commons

Yu-Hui Lin<sup>1</sup> and Joshua S. Weitz<sup>1,2</sup>

<sup>1</sup>*School of Physics, Georgia Institute of Technology, Atlanta, GA, USA*

<sup>2</sup>*School of Biological Sciences, Georgia Institute of Technology, Atlanta, GA, USA*

(Dated: January 23, 2019)

A tragedy of the commons (TOC) occurs when individuals acting in their own self-interest deplete commonly-held resources, leading to a worse outcome than had they cooperated. Over time, the depletion of resources can change incentives for subsequent actions. Here, we investigate long-term feedback between game and environment across a continuum of incentives in an individual-based framework. We identify payoff-dependent transition rules that lead to oscillatory TOC-s in stochastic simulations and the mean field limit. Further extending the stochastic model, we find that spatially explicit interactions can lead to emergent, localized dynamics, including the propagation of cooperative wave fronts and cluster formation of both social context and resources. These dynamics suggest new mechanisms underlying how TOCs arise and how they might be averted.

In 1968, Garrett Hardin explored a social dilemma, which he termed the ‘Tragedy of the Commons’ (TOC) [1]. The social dilemma arises when two individuals choose amongst distinct strategies to utilize a limited public good. Both individuals receive the maximal combined benefit if they utilize the public good with restraint, i.e., if they ‘cooperate’. However, each individual receives the maximal personal benefit if they utilize the public good without restraint, i.e., if they ‘defect’, while their opponent cooperates. As a consequence, individuals acting rationally will cheat leaving all worse off. Hardin argued that such a TOC is inevitable [1].

Evolutionary dynamics arising from a TOC dilemma can be modeled in terms of changes in the frequencies of individuals from two populations. Individuals interact and receive payoffs that depend on their strategy and the strategy of their opponent. In replicator dynamics [2], the payoff represents a relative fitness which determines the growth of cooperators, with frequency  $x$ , and of defectors, with frequency  $1 - x$ , i.e.,:

$$\dot{x} = x(1-x)(r_C(x, A) - r_D(x, A)). \quad (1)$$

The values  $r_C$  and  $r_D$  denote the context-dependent fitness payoff to cooperators and defectors respectively, given the payoff matrix [3],  $A = \begin{bmatrix} R & S \\ T & P \end{bmatrix}$ , where  $r_C = Rx + S(1-x)$ ,  $r_D = Tx + P(1-x)$  and where  $R$  denotes the reward to cooperation,  $T$  denotes the temptation to cheat,  $S$  denotes the sucker’s payoff, and  $P$  denotes the punishment given mutual defection. A TOC occurs when  $T > R$ ,  $P > S$ , and  $P < R$ . However, in contrast to standard game theory assumptions, payoffs are unlikely to remain fixed after repeated decisions that degraded commonly-held resources.

To address this issue, a recent model [4] considered dynamics arising given resource-dependent payoff matrices  $A(n) = A_0(1-n) + A_1(n)$ , which interpolate between  $A_0$  and  $A_1$ , the payoff matrices given deplete and replete resource states, respectively, i.e.,  $A(n) = \begin{bmatrix} R_0 & S_0 \\ T_0 & P_0 \end{bmatrix} (1-n) + \begin{bmatrix} R_1 & S_1 \\ T_1 & P_1 \end{bmatrix} n$ . This model of coevolutionary game dynamics included feedback with the environmen-

tal state denoted by  $0 \leq n \leq 1$ , such that

$$\epsilon \dot{x} = x(1-x)[r_C(x, A(n)) - r_D(x, A(n))], \quad (2)$$

$$\dot{n} = n(1-n)(\theta x - (1-x)). \quad (3)$$

where  $\epsilon$  is a speed parameter and  $\theta$  denotes the strength of cooperators in restoring the environment. In this coevolutionary model, the payoff matrices  $A_0$  and  $A_1$  can have markedly different Nash equilibria [5]. For example, when defection is uniformly favored when  $n = 1$  and cooperation is favored when  $n = 0$ , then the the system can exhibit a novel phenomenon termed an ‘oscillatory tragedy of the commons’ (o-TOC). An o-TOC denotes a trajectory in the phase plan that approaches a heteroclinic cycle. Given a replete environment, the population rapidly switches from cooperation to defection, which then degrades the environment. In the depleted environment, cooperators re-establish, improving the environment, then defectors invade and the cycle repeats. Other outcomes, including a TOC and the aversion of a TOC can emerge given other payoff matrices [4].

This coevolutionary game model is the basis for our development and analysis of an individual-based framework to assess the influence of noise (first) and spatially explicit interactions (second) on the emergent dynamics of social context and resources. To begin, consider a system comprised of  $N_C$  cooperators and  $N_D$  defectors, such that  $N = N_C + N_D$ . A single time step consists of  $N$  events. In each event, a randomly chosen individual (the focal player) interacts with another individual (the opponent) chosen at random. The payoff to the focal player influences its probability to reproduce. Critically in our proposed framework, successful reproduction by the focal player replaces a randomly chosen *third* individual (see [6] for a related public goods model that decouples interaction and reproduction). The following reactions denote those transitions that lead to a change

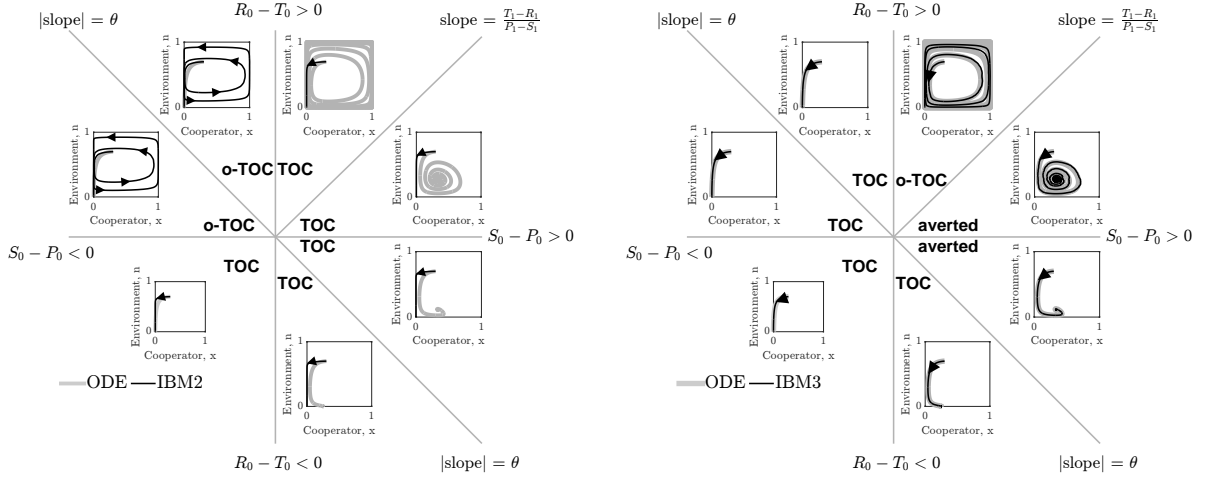
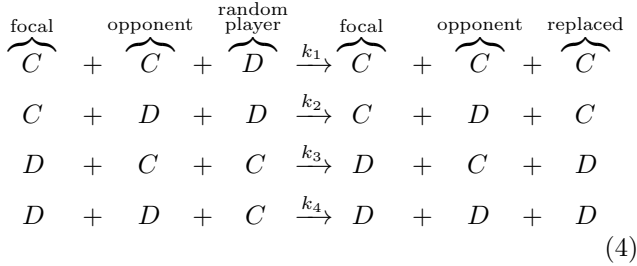


FIG. 1. Coevolutionary dynamics of strategies and resources in replicator and IBM dynamics. (a) The dynamics with IBM2, in which offspring of the focal player replace the opponent. (b) The dynamics with IBM3, in which offspring of the focal player replaces a random individual. In both panels, parameter space is divided according to the sign of  $R_0 - T_0$ ,  $S_0 - P_0$ . In each section in the parameter space, a phase diagram with different  $A_0$  in is shown, where the x-axis represents  $x$  and the y-axis denotes  $n$ . Light gray trajectories are mean field solutions and black trajectories denote IBM dynamics where arrows denote the flow of time. Visualized IBM trajectories are the average of 100 replicates with the same parameter set, except for oscillatory dynamics, given phase differences that can arise due to demographic noise. Common parameters for all replicates:  $\theta = 2$ ,  $\epsilon = 0.5$ ,  $\Delta x = 1$ , and  $\Delta t = 0.05$ ,  $A_1 = [3, 0; 5, 1]$ ;  $A_0$  varies by region. Full parameter list for  $A_0$  in FIG. S1.

in the number of cooperators or defectors:



where  $k_i$  denote reproduction rates.

In the three-individual framework, the master equation for the dynamics of cooperators is:

$$\begin{aligned}
 \mathbb{P}(n_C, \tau + \Delta\tau) &= \mathbb{P}(n_C, \tau) + \mathbb{T}(n_C | n_C - 1) \mathbb{P}(n_C - 1, \tau) \Delta\tau \\
 &\quad + \mathbb{T}(n_C | n_C + 1) \mathbb{P}(n_C + 1, \tau) \Delta\tau \\
 &\quad - \mathbb{T}(n_C + 1 | n_C) \mathbb{P}(n_C, \tau) \Delta\tau \\
 &\quad - \mathbb{T}(n_C - 1 | n_C) \mathbb{P}(n_C, \tau) \Delta\tau + \mathcal{O}(\Delta\tau^2),
 \end{aligned} \quad (5)$$

where the transition rates are:

$$\begin{aligned}
 \mathbb{T}(n_C + 1 | n_C) &= k_1 n_C \frac{n_C - 1}{N - 1} \frac{n_D}{N - 1} + k_2 n_C \frac{n_D}{N - 1} \frac{n_D}{N - 1} \\
 \mathbb{T}(n_C - 1 | n_C) &= k_3 n_D \frac{n_C}{N - 1} \frac{n_C}{N - 1} + k_4 n_D \frac{n_D - 1}{N - 1} \frac{n_C}{N - 1}.
 \end{aligned} \quad (6)$$

In the SI, we derive the expected mean field dynamics for the frequency of cooperators  $x \equiv \lim_{N, n_c \rightarrow \infty} \left( \frac{n_c}{N} \right)$  from the master equation:

$$\dot{x} = x(1-x) [(k_1 - k_3)x + (k_2 - k_4)(1-x)]. \quad (7)$$

We recover the replicator dynamics of the coevolutionary model when  $k_1 = R(n)$ ,  $k_2 = S(n)$ ,  $k_3 = T(n)$ , and  $k_4 = P(n)$ . Hence, transition rates are a function of resource- and social-context dependent payoffs. In contrast, mean field dynamics derived via a two-player individual based model formulation (IBM2) result in a logistic dependency on  $x$  distinct from the cubic nonlinearity in Eq. 7 (see SI for derivation and details).

In order to further evaluate stochastic dynamics of the IBM formulation, we simulated the joint dynamics of resources  $n$  and social context  $x$  using  $N = 10^4$  individuals. A single time step over an interval  $\Delta t$  includes  $N$  game steps followed by changes in resource levels,  $n(t)$  according to Eq. 3 (see Supplementary Information (SI) for details). Given the master equation analysis, we define reproduction rates  $k_i$  based on the current environmental state  $n(t)$ . Consistent with our finding from the master equation, the simulation results of the individual-based model involving three players (IBM3) recapitulate predictions of the mean-field replicator dynamics model (see FIG. 1-right). Specifically, we identify seven distinct phases corresponding to the relative magnitude of payoffs given the resource deplete state. The phases and their asymptotic behavior agree qualitatively with mean-field predictions. In contrast, if the focal player reproduces and replaces the opponent (as is often assumed in two-player variants of spatial games), then the individual-based simulations diverge from predictions (see FIG. 1-left) as anticipated from expected mean field dynamics (see SI).

There are two notable quantitative differences in the IBM3 simulations with respect to predictions from repli-

cator dynamics. First, whereas mean-field dynamics predict convergence to a heteroclinic cycle (see ‘o-TOC’ region in FIG. 1-right), the IBM simulations stochastically reach an absorbing state on the boundary. Such a result is anticipated in any finite size simulation, given that heteroclinic cycles asymptotically approach the boundary. Second, the mean field model predicts closed period orbits given certain symmetric properties of  $A_0$  and  $A_1$  (corresponding to the line with slope  $(T_1 - R_1)/(P_1 - S_1)$  in FIG. 1-right.) In contrast, the IBM simulations have demographic noise, which can lead to repeated oscillations and convergence to a boundary (see FIG. S3).

To study the combined effects of spatial structure and demographic noise (see [7]) we extended the IBM3 framework a 2-dimensional fully occupied lattice with  $L$  sites per dimension given periodic boundary conditions, where the  $N = L^2$  individuals are either cooperators or defectors. The focal player is selected at random and opponent is chosen randomly from the von Neumann neighborhood of the focal player. We denote the position of the focal player (opponent) as  $\vec{r}_F$  ( $\vec{r}_O$ ). The focal player reproduces with probability rate  $k_m(s_F, s_O, \bar{n})$  given the strategy set of focal player and opponent,  $s_F$  and  $s_O$ , and the average local environment,  $\bar{n} = (n(\vec{r}_F) + n(\vec{r}_O))/2$ . Environmental state dynamics  $n(\vec{r}, t)$  are augmented by diffusion, i.e.,:

$$\frac{\partial n}{\partial t} = n(1 - n)(\theta x - (1 - x)) + D_n \nabla^2 n. \quad (8)$$

The diffusivity  $D_n$  controls the redistribution of resources relative to population dynamics.

Simulations of coevolutionary game-environmental dynamics reveal dramatic changes in outcomes given spatially explicit interactions. FIG. 2 compares dynamics of non-spatial and spatial IBM models with three different diffusivities,  $D_n = 0, 1, \infty$ , classifying outcomes based on whether there is a TOC or not (the latter we term averted, see SI for criteria). The heat maps show the proportion of averted cases among all replicates. Spatial interactions enable TOC aversion when cooperation is favored given a coordination game context ( $R_0 > T_0$  and  $S_0 < P_0$ , see upper left). However, spatial interactions also restrict the parameter regimes where a TOC can be averted given an anti-coordination game context ( $R_0 < T_0$  and  $S_0 > P_0$ , see bottom right). For long-term dynamics, we find that oscillating dynamics are typical in  $D_n = \infty$  cases (see examples in the SI). Such oscillatory dynamics can spiral inwards when TOC-s are averted or outwards to the boundary. Of note, amongst IBM models we only observe a persistent o-TOC when  $D_n = \infty$ ; indicating the role of strong spatial coupling to induce oscillations.

We further investigated spatiotemporal dynamics focusing on variation in  $D_n$  given parameter regimes with both averted and TOC dynamics. These regimes correspond to the case where  $S_0 < P_0$ ,  $R_0 > T_0$  and where  $R_0 > -\theta(S_0 - P_0) + T_0$  (see bottom panels of FIG. 2). The results of spatially explicit IBM3 model simulations

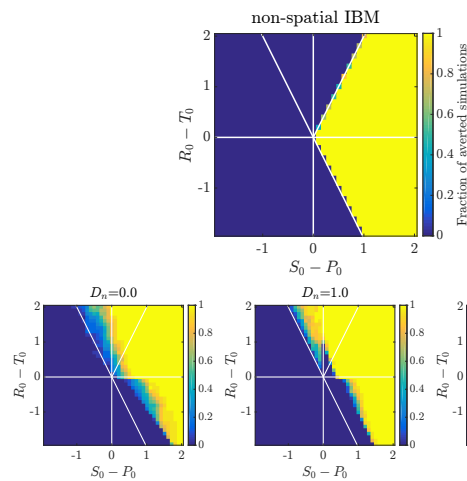


FIG. 2. Strategy-resource dynamics given spatial interactions. Colors in each heat-map denote the fraction of averted dynamics out of 20 replicates with different  $A_0$ 's. The horizontal axis of the heat maps are  $S_0 - P_0$  and the vertical ones are  $R_0 - T_0$ . Each grid on the heat maps has increment 0.1. The diffusivity  $D_n$  is showed in the title of each panel. Other parameters for all replicates are  $L = 100$ ,  $\theta = 2$ ,  $\epsilon = 0.5$ ,  $\Delta x = 1$ , and  $\Delta t = 0.05$ ,  $A_1 = [3, 0; 5, 1]$ . The white lines mark out the boundary of different dynamics predicted by the mean field model. Full parameter list for  $A_0$  in each regime are listed in FIG. S2.

are shown in FIG. 3 for  $D_n = 0, 1$  and  $\infty$ . Notably, all cases appear to exhibit clustering amongst cooperators and the cases with heterogeneous environmental dynamics ( $D_n = 0$  and  $D_n = 1$ ) also appear to exhibit clustering between cooperators and environmental resource state. However, there are markedly different types of emergent spatial patterns give variation in the diffusivity of environmental resource state. In order to assess clustering quantitatively, we analyzed the joint structure of social context and resource levels by measuring the spatial cross-correlation function:

$$g_{CN}(r, t) = \frac{L^2}{\mathcal{A}(r)} \frac{\sum_{i,j} (\sum_{i',j'} x_{i,j}(t) \cdot n_{i',j'}(t))}{\sum_{i,j} x_{i,j}(t) \sum_{i,j} n_{i,j}(t)}, \quad (9)$$

and the spatial autocorrelation function of cooperator clustering:

$$g_{CC}(r, t) = \frac{L^2}{\mathcal{A}(r)} \frac{\sum_{i,j} (\sum_{i',j'} x_{i,j}(t) \cdot x_{i',j'}(t))}{(\sum_{i,j} x_{i,j}(t))^2}, \quad (10)$$

where  $r < \sqrt{(i - i')^2 + (j - j')^2} \leq r + 1$ , and  $\mathcal{A}(r)$  denotes the number of lattice sites within this range in both cases. We then fit the short-range components of the observed correlation at a fixed time point to a decaying exponential, i.e.,  $g(r, t) \sim 1 + \alpha(t)e^{-r/\xi(t)}$  given pre-factor  $\alpha$  and correlation length  $\xi$ . We then fit the short-range components of the observed correlation at a fixed time point to a decaying exponential, i.e.,  $g(r, t) \sim 1 + \alpha(t)e^{-r/\xi(t)}$  given pre-factor  $\alpha$  and correlation length  $\xi$ . The spatial autocorrelation analysis confirms the emergence of clustering amongst cooperators when the TOC is averted,

i.e.,  $g_{CC}(r) > 1$  for  $r \rightarrow 1$  (see black lines in the sub-panels of FIG. 3). Yet there are marked differences in the dynamics of the cross-correlation between cooperators and the environmental state.

For  $D_n = 0$ , the environment and cooperative population propagate outward as a wave. The cooperative population spread leaving patches of resource replete environments. The  $g_{CN}(r)$  plots shows that  $x$  and  $n$  can be positively correlated as a wave initiates but negatively correlated once defectors invade and replace resource replete environments, leading to (often disjoint) patchy distributions of both resources and cooperators. In contrast, for  $D_n = 1$ , small clusters of cooperators and localized resources form after initial transient dynamics. This feature is captured by the  $g_{CN}(r)$  analysis, revealing strongly elevated cross-correlation (see the middle row of FIG. 3) as well as similar pattern in the dynamics of  $g_{CC}(r)$  and  $g_{CN}(r)$ . We note that these ‘gangs’ of cooperators and their environmental ‘tail’ are chased by a dominant group of defectors (see [8] for related findings in evolutionary PD models without environmental feedback). Finally, given  $D_n = \infty$ , the resources are uniform across space. Cooperative clusters grow towards system sizes due to the strong spatial coupling mediated via fast resource diffusivity. The single large cooperator cluster expands and shrinks over time with increasing amplitude, as evidenced by the elevated autocorrelation of  $g_{CC}(r)$  in the bottom row of FIG. 3, with rapid switches in resource state, leading to an eventual collapse of the cooperator population. We do not report  $g_{CN}(r)$  given the uniform distribution of resources given  $D_n = \infty$ .

In summary, we have developed an individual-based framework to incorporate the analysis of demographic noise and spatial interactions in coevolutionary game dynamics that coupled individual strategies and the environment [7]. The IBM involving 3 players in a game recapitulates and generalizes earlier findings from a coevolutionary game model, including the emergence of an oscillatory tragedy of the commons. Spatial interactions can shift the domains in which a tragedy of the commons may arise when compared to non-spatial models [9]. Spatially explicit dynamics also lead to novel, coherent spatiotemporal patterns [10–14], including diffusive clusters, flickering, and wave-like patterns. These joint dynamics of resources and social strategies suggest multiple avenues for future study, including formally deriving effective PDEs to characterize whether the system permits propagating waves in the large system limit. It will also be critical to evaluate the extent to which spatial interactions modify strategy-environment feedback in proposed generalizations [15] of the replicator framework underlying the present work [4] and in stochastic games with feedback between behavior and public good states [16]. Finally, the spatial approach may also aid efforts to understand how microorganisms produce and utilize public goods, *e.g.*, siderophores – extracellular iron harvesting enzymes [6, 17–20]. Given increasing pressures on limited resources, we intend to leverage prior

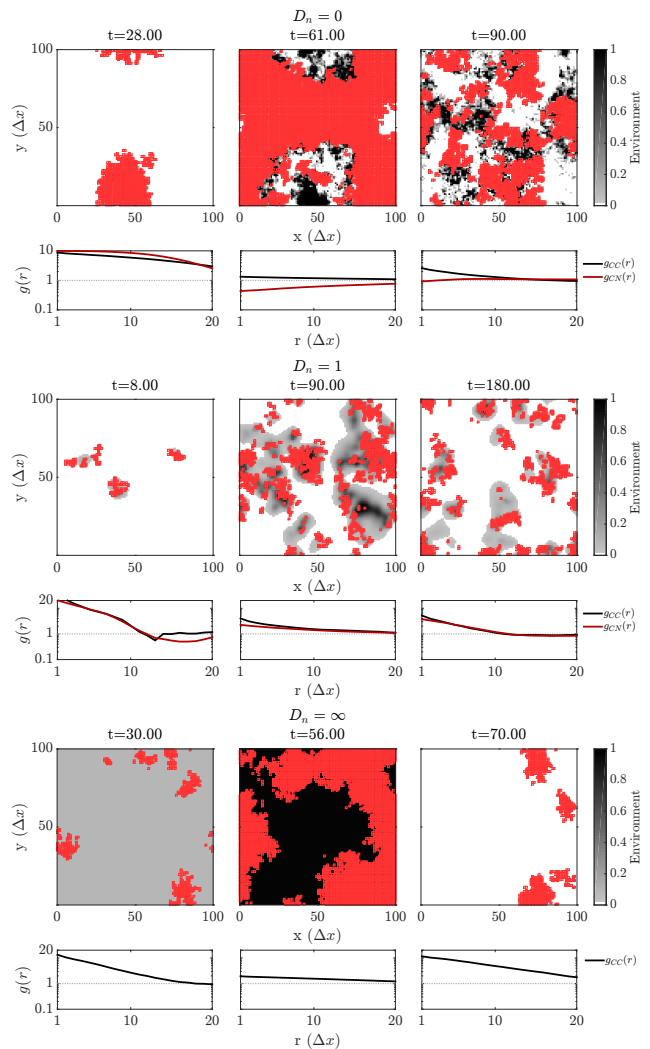


FIG. 3. Spatiotemporal dynamics of resources and cooperation. The background color represents the environment, while a red square means a cooperator occupy the lattice site. The empty sites are occupied by defectors. (Top row)  $D_n = 0$ , a circular wave of cooperative population propagates outward. (Middle row)  $D_n = 1$ , a few small patches of cooperators move around and divide. (Bottom row)  $D_n = \infty$ , a large cooperator cluster expand and shrink over time with increasing amplitude until extinction.

work on controlling mean-field strategy-environment dynamics [21] to identify ways in which local manipulation of resources, strategies, and/or perceptions can help stabilize and conserve the commons.

## ACKNOWLEDGEMENTS

We thank Erol Akçay, Marianne Bauer, Ceyhan Eksin, Guanlin Li, Keith Paarporn, William Ratcliff, and Peter Yunker for feedback and Stephen Beckett for reviewing code. This work was supported by the Simons Foundation (SCOPE award ID 329108, J.S.W.) and by Army Research Office grant W911NF-14-1-0402.

- 
- [1] G. Hardin, *Science* **162**, 1243 (1968).
- [2] M. A. Nowak, *Evolutionary Dynamics* (Harvard University Press, 2006).
- [3] J. M. Smith and G. R. Price, *Nature* **246**, 15 (1973).
- [4] J. S. Weitz, C. Eksin, K. Paarporn, S. P. Brown, and W. C. Ratcliff, *Proceedings of the National Academy of Sciences* **113**, E7518 (2016).
- [5] J. F. Nash Jr, *Econometrica: Journal of the Econometric Society* , 155 (1950).
- [6] M. Bauer and E. Frey, *Physical Review E* **97**, 042307 (2018).
- [7] R. Durrett and S. Levin, *Theoretical Population Biology* **46**, 363 (1994).
- [8] G. Szabó and C. Tóke, *Physical Review E* **58**, 69 (1998).
- [9] J. Halatek and E. Frey, *Nature Physics* **14**, 507 (2018).
- [10] M. A. Nowak and R. M. May, *Nature* **359**, 826 (1992).
- [11] T. Butler and N. Goldenfeld, *Physical Review E* **80**, 030902 (2009).
- [12] T. Butler and N. Goldenfeld, *Physical Review E* **84**, 011112 (2011).
- [13] M. A. Nowak and R. M. May, *International Journal of Bifurcation and Chaos* **3**, 35 (1993).
- [14] M. Nanda and R. Durrett, *Proceedings of the National Academy of Sciences* **114**, 6046 (2017).
- [15] A. R. Tilman, E. Akçaya, and J. Plotkin, *bioRxiv* (2018), 10.1101/493023.
- [16] C. Hilbe, Š. Šimsa, K. Chatterjee, and M. A. Nowak, *Nature* **559**, 246 (2018).
- [17] O. X. Cordero, L.-A. Ventouras, E. F. DeLong, and M. F. Polz, *Proceedings of the National Academy of Sciences* **109**, 20059 (2012).
- [18] R. Niehus, A. Picot, N. M. Oliveira, S. Mitri, and K. R. Foster, *Evolution* **71**, 1443 (2017).
- [19] R. Menon and K. S. Korolev, *Physical Review Letters* **114**, 168102 (2015).
- [20] O. Lewin-Epstein, R. Aharonov, and L. Hadany, *Nature Communications* **8**, 14040 (2017).
- [21] K. Paarporn, C. Eksin, J. S. Weitz, and Y. Wardi, *arXiv preprint arXiv:1803.06737* (2018).

**Supplementary information for the manuscript**  
**“Spatial interactions and oscillatory tragedies of the commons”**

Yu-Hui Lin<sup>1</sup> and Joshua S. Weitz<sup>1,2</sup>

<sup>1</sup>*School of Physics, Georgia Institute of Technology, Atlanta, GA, USA*

<sup>2</sup>*School of Biological Sciences, Georgia Institute of Technology, Atlanta, GA, USA*

(Dated: January 23, 2019)

**I. DERIVATION OF INDIVIDUAL GAME RULES RECOVERING REPLICATOR DYNAMICS**

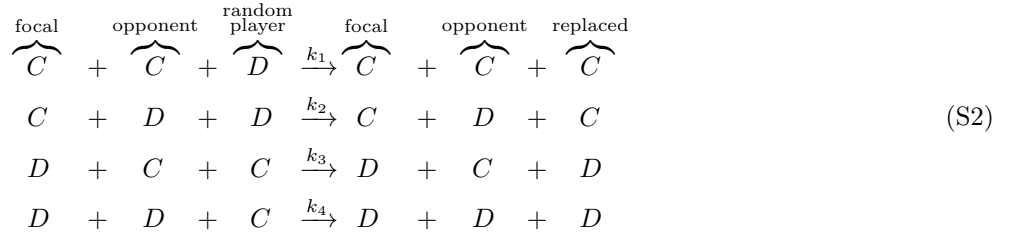
Here we derive the individual based game rules that are able to recover replicator dynamics

$$x' = x(1-x)(r_C(x,n) - r_D(x,n)), \quad (S1)$$

in the continuous limit. The time is scaled by parameter  $\epsilon$  for more compact expression. The normalized time  $\frac{t}{\epsilon}$  will be denoted as  $\tau$  hereafter. We express the time derivation with respect to normalized time with the prime symbol. We postulate that individuals undergo a birth-death process: a focal player that wins against its opponent in a game can reproduce a new individual with the same strategy and replace (A) another random player in the system or (B) the opponent. Here we show the derivation process of the scenario where a game involves three players (A), which recapitulates the form of replicator dynamics first. The derivation following similar process but with only 2 individuals involved in a game will be briefly introduced after derivation of (A) to show how it fails.

**A. Individual-based rules involving 3 players in a game**

We write the events in a chemical reaction form with reaction rates  $k_i$ . The total number of players in the system is constant as a result of the birth-death process,  $N = n_C + n_D$ , where  $n_C$  and  $n_D$  stand for number of cooperators and defectors respectively. With  $C$  denoting a cooperator and  $D$  denoting a defector, the possible combinations of players involved in a game are



The transition rates of Eq. S2 are

$$\begin{aligned}
 \mathbb{T}(n_C + 1 | n_C) &= k_1 \cdot n_C \cdot \overbrace{\frac{n_C - 1}{N - 1}}^{\text{randomly choosing an opponent C}} \cdot \overbrace{\frac{n_D}{N - 1}}^{\text{a random D to be replaced}} + k_2 \cdot n_C \cdot \overbrace{\frac{n_D}{N - 1}}^{\text{randomly choosing an opponent D}} \cdot \overbrace{\frac{n_D}{N - 1}}^{\text{a random D to be replaced}} \\
 \mathbb{T}(n_C - 1 | n_C) &= k_3 \cdot n_D \cdot \overbrace{\frac{n_C}{N - 1}}^{\text{randomly choosing an opponent C}} \cdot \overbrace{\frac{n_C}{N - 1}}^{\text{a random C to be replaced}} + k_4 \cdot n_D \cdot \overbrace{\frac{n_D - 1}{N - 1}}^{\text{randomly choosing an opponent D}} \cdot \overbrace{\frac{n_C}{N - 1}}^{\text{a random C to be replaced}}.
 \end{aligned} \quad (S3)$$

The terms in the above equations describe the change in number of two types of players in a probabilistic perspective: there are  $n_C$  ( $n_D$ ) cooperators (defectors) in the system, each of which has probability to pick another player, either a cooperator ( $\frac{n_C-1}{N-1}$ ) or a defector ( $\frac{n_D-1}{N-1}$ ), as an opponent. At each time increment, the focal player can produce a new individual with reaction rate  $k_i \Delta \tau$ . All players other than the focal player in the system has equal chance to be replaced by the newborn individual. The individual to be replaced is a cooperator (defector) with probability  $\frac{n_C-1}{N-1}$

$(\frac{N_D-1}{N-1})$ . Combining the transition probability of all the possible events listed above, the master equation that governs the change in  $n_C$  is accordingly

$$\begin{aligned} \mathbb{P}(n_C, \tau + \Delta\tau) &= \mathbb{P}(n_C, \tau) + \mathbb{T}(n_C|n_C - 1)\mathbb{P}(n_C - 1, \tau)\Delta\tau + \mathbb{T}(n_C|n_C + 1)\mathbb{P}(n_C + 1, \tau)\Delta\tau \\ &\quad - \mathbb{T}(n_C + 1|n_C)\mathbb{P}(n_C, \tau)\Delta\tau - \mathbb{T}(n_C - 1|n_C)\mathbb{P}(n_C, \tau)\Delta\tau + \mathcal{O}(\Delta\tau^2). \end{aligned} \quad (\text{S4})$$

Rearranging the master equation Eq. S4, dividing both side by  $\Delta\tau$  and taking  $\Delta\tau$  to be infinitesimal yields

$$\begin{aligned} \mathbb{P}'(n_C, \tau) &= \mathbb{T}(n_C|n_C - 1)\mathbb{P}(n_C - 1, \tau) + \mathbb{T}(n_C|n_C + 1)\mathbb{P}(n_C + 1, \tau) \\ &\quad - \mathbb{T}(n_C + 1|n_C)\mathbb{P}(n_C, \tau) - \mathbb{T}(n_C - 1|n_C)\mathbb{P}(n_C, \tau). \end{aligned} \quad (\text{S5})$$

To examine if the master equation derived from the individual-based events recovers replicator dynamics in the continuous limit, we need to derive the time differential equation of the expected value of  $n_C$  from the master equation Eq. S5. To proceed, we denote the expected value of a variable with angular brackets. The definition of the expected value of a random variable  $X$  is

$$\langle X(\tau) \rangle = \sum_X X\mathbb{P}(X, \tau). \quad (\text{S6})$$

Next, we multiply each term in the master equation Eq. S5 with  $n_C$  and sum over all possible values of  $n_C$  to obtain the time differential equation describing the dynamics of  $\langle n_C \rangle$ .

$$\begin{aligned} \sum_{n_C=0}^N n_C \mathbb{P}'(n_C) &= \sum_{n_C=1}^N n_C \mathbb{T}(n_C|n_C - 1)\mathbb{P}(n_C - 1) + \sum_{n_C=0}^{N-1} n_C \mathbb{T}(n_C|n_C + 1)\mathbb{P}(n_C + 1) \\ &\quad - \sum_{n_C=0}^N n_C \mathbb{T}(n_C + 1|n_C)\mathbb{P}(n_C) - \sum_{n_C=0}^N n_C \mathbb{T}(n_C - 1|n_C)\mathbb{P}(n_C) \\ &= \sum_{n_C=0}^N (n_C + 1)\mathbb{T}(n_C + 1|n_C)\mathbb{P}(n_C) + \sum_{n_C=0}^N (n_C - 1)\mathbb{T}(n_C - 1|n_C)\mathbb{P}(n_C) \\ &\quad - \sum_{n_C=0}^N n_C \mathbb{T}(n_C + 1|n_C)\mathbb{P}(n_C) - \sum_{n_C=0}^N n_C \mathbb{T}(n_C - 1|n_C)\mathbb{P}(n_C) \\ &= \sum_{n_C=0}^N \mathbb{T}(n_C + 1|n_C)\mathbb{P}(n_C) - \sum_{n_C=0}^N n_C \mathbb{T}(n_C - 1|n_C)\mathbb{P}(n_C). \end{aligned} \quad (\text{S7})$$

Plugging the expressions of transition rates in eq. Eq. S3 into the last equation Eq. S7 leads to

$$\begin{aligned} \langle n_C \rangle' &= \langle \mathbb{T}(n_C + 1|n_C) \rangle - \langle \mathbb{T}(n_C - 1|n_C) \rangle \\ &\approx k_1 \cdot \langle n_C \cdot \frac{n_C}{N} \cdot \frac{n_D}{N} \rangle + k_2 \cdot \langle n_C \cdot \frac{n_D}{N} \cdot \frac{n_D}{N} \rangle - k_3 \cdot \langle n_D \cdot \frac{n_C}{N} \cdot \frac{n_C}{N} \rangle - k_4 \cdot \langle n_D \cdot \frac{n_C}{N} \cdot \frac{n_D}{N} \rangle. \end{aligned} \quad (\text{S8})$$

when  $N, n_C, n_D \gg 1$ . As stated earlier,  $N = n_C + n_D$  is a constant in the system. We then define  $x \equiv \frac{n_C}{N}$ , and thus  $\frac{n_D}{N} = 1 - x$ . Dividing both sides of Eq. S8 by  $N$ , we find

$$\langle x \rangle' = k_1 \cdot \langle x^2(1 - x) \rangle + k_2 \cdot \langle x(1 - x)^2 \rangle - k_3 \cdot \langle x^2(1 - x) \rangle - k_4 \cdot \langle x(1 - x)^2 \rangle. \quad (\text{S9})$$

For sufficiently large populations, fluctuations around the average value are expected to be sufficiently small, and by ignoring correlatinos, we approximate the expected values with actual values and omit the angular brackets. Rearranging Eq. S10 and omitting angular brackets, we get

$$x' = x(1 - x)[(k_1x + k_2(1 - x)) - (k_3x + k_4(1 - x))], \quad (\text{S10})$$

which recovers replicator dynamics with growth rates

$$\begin{bmatrix} r_C \\ r_D \end{bmatrix} = \begin{bmatrix} k_1 & k_2 \\ k_3 & k_4 \end{bmatrix} \begin{bmatrix} x \\ 1 - x \end{bmatrix} = \begin{bmatrix} k_1x + k_2(1 - x) \\ k_3x + k_4(1 - x) \end{bmatrix}.$$

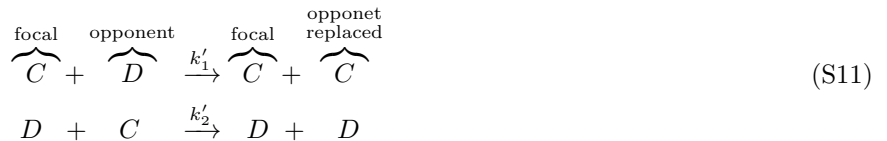
Compared with Eq. 2 in the main text, it is apparent that the values of  $k_i$ 's should be

$$\begin{cases} k_1 = R(n) \\ k_2 = S(n) \\ k_3 = T(n) \\ k_4 = P(n) \end{cases}.$$

which correspond to the payoffs of focal players.

### B. Individual-based rules involving 2 players in a game

Interactions between individuals in a chemical equation form with reaction rates  $k_i$  are



Transition rates of Eq. S11 are

$$\begin{aligned} \mathbb{T}(n_C + 1|n_C) &= k'_1 \cdot n_C \cdot \overbrace{\frac{n_D}{N-1}}^{\text{randomly choosing an opponent C}} \\ \mathbb{T}(n_C - 1|n_C) &= k'_2 \cdot n_D \cdot \overbrace{\frac{n_C}{N-1}}^{\text{randomly choosing an opponent C}}. \end{aligned} \quad (\text{S12})$$

Following the same derivation from Eq. S5 to Eq. S7 and plugging the expressions of transition rates in Eq. S12,

$$\begin{aligned} \langle n_C \rangle' &= \langle \mathbb{T}(n_C + 1|n_C) \rangle - \langle \mathbb{T}(n_C - 1|n_C) \rangle \\ &\approx k'_1 \cdot \langle n_C \cdot \frac{n_D}{N} \rangle - k'_2 \cdot \langle n_D \cdot \frac{n_C}{N} \rangle, \end{aligned} \quad (\text{S13})$$

when  $N, n_C, n_D \gg 1$ . As before,  $N = n_C + n_D$  is a constant in the system. We define  $x \equiv \frac{n_C}{N}$  and thus  $\frac{n_D}{N} = 1 - x$ . Dividing both sides of Eq. S13 gives

$$\langle x \rangle' = k'_1 \cdot \langle x(1-x) \rangle - k'_2 \cdot \langle x(1-x) \rangle. \quad (\text{S14})$$

For large populations, the fluctuations around expected values are negligible, and by assuming the absence of higher-order correlation, we find

$$x = (k'_1 - k'_2)x(1-x). \quad (\text{S15})$$

This mean field dynamics in the IBM2 model is quadratic in  $x$  assuming  $k_i$ 's do not depend on information other than payoffs, rather than being cubic in  $x$  as expected in the replicator dynamics for the IBM3 model.

## II. SIMULATION DETAILS

### A. Individual-based simulation

To simulate the coevolutionary dynamics in an individual-based, game-theoretic perspective, we adopt the individual-based game rules derived in section IA. We simulate  $N$  games sequentially to allow equal chance of each individual to be involved in a game within a time step  $\Delta t$ . At the beginning of each time step, each player is labelled by an integer ranging from 1 to  $N$ . 3 randomly permuted number series ranging from 1 to  $N$  are generated. The  $i$ -th elements in the three random number series represent the index of the focal player, the opponent, the individual to be

replaced in the  $i$ -th game respectively. A random number  $r \in [0, 1)$  is generated for each game, and the birth-death process happens if  $r > k_i \Delta \tau = k_i \frac{\Delta t}{\epsilon}$ .  $k_i$  is the reaction rate and depends on the strategies of the focal player and the opponent. We complete a time step by updating environment  $n$  with Euler method,

$$\Delta n = \dot{n} \Delta t = n(1 - n)(\theta x_{new}(t) - (1 - x_{new}(t))) \Delta t,$$

after  $N$  games. The subscript *new* denotes that the value of  $x$  in  $\dot{n}$  is taken to be the one after  $N$  games, rather than the value at the beginning of the simulation time step. A simulation proceeds to the next time step after both  $x$  and  $n$  are updated, and stops when total number of time steps reaches an assigned simulation horizon.

## B. Spatially-explicit simulation

We perform spatially-explicit simulations on a 2D  $L \times L$  lattice. Each lattice site can only be occupied by a single player, either a cooperator or a defector. The rules for updating individual strategy in spatially-explicit simulations are similar to that in non-spatial simulations. Instead of generating three random number series, only a randomly permuted number series is generated to represent the index of the focal player in each game. The opponent player and the individual to be replaced are then chosen in the von Neumann neighborhood of the focal player.

After  $N$  sequential games, the spatial profile of the environment is updated in two steps.

$$n_{i,j,s}(t) = n_{i,j}(t) + n_{i,j}(t)(1 - n_{ij}(t)) (\theta x_{i,j,new} - (1 - x_{i,j,new})) \quad (\text{S16a})$$

$$n_{i,j,f}(t + \Delta t) = \begin{cases} D_n \frac{\Delta t}{\Delta x^2} (n_{i-1,j,s}(t) - 2n_{i,j,s}(t) + n_{i+1,j,s}(t) \\ \quad + n_{i,j-1,s}(t) - 2n_{i,j,s}(t) + n_{i,j+1,new}(t)) , & \text{for } D_n = 0 \text{ or } 1 \\ \frac{\Sigma_{i,j} n_{i,j,s}(t)}{L \cdot L}, & \text{for } D_n = \infty \end{cases} \quad (\text{S16b})$$

The first step (Eq. S16a) accounts for change in  $n$  due to individual strategies adopted in previous games in the same time step. The second step accounts for diffusion was calculated with standard explicit forward-time centered-space method (Eq. S16b). The subscripts  $i, j$  denote the value at coordinate  $(i, j)$ . The subscript *new* in  $x_{new}$  again denotes the updated quantity after  $N$  games.  $s$  in  $n_{i,j,s}$  means the value of  $n$  is only affected by the individual strategies but has not yet accounted for the effect of diffusion.  $f$  in  $n_{i,j,f}$  indicates this is the final value for  $n$  after a time step  $\Delta t$ . As before, a spatial simulation proceeds to the next simulation step after both  $x$  and  $n$  are updated and stops at some pre-assigned simulation horizon.

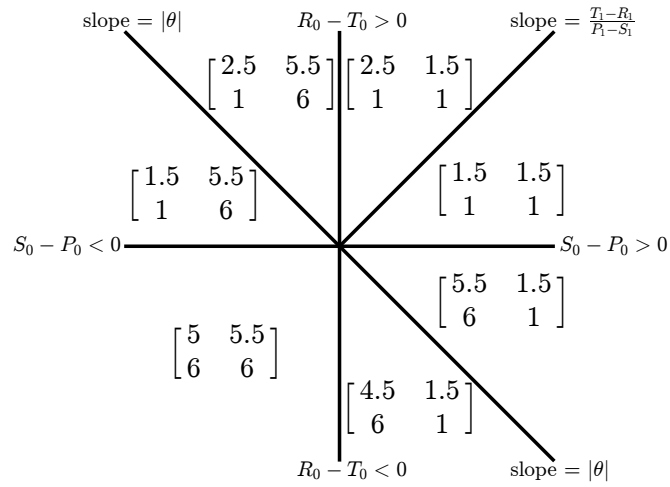
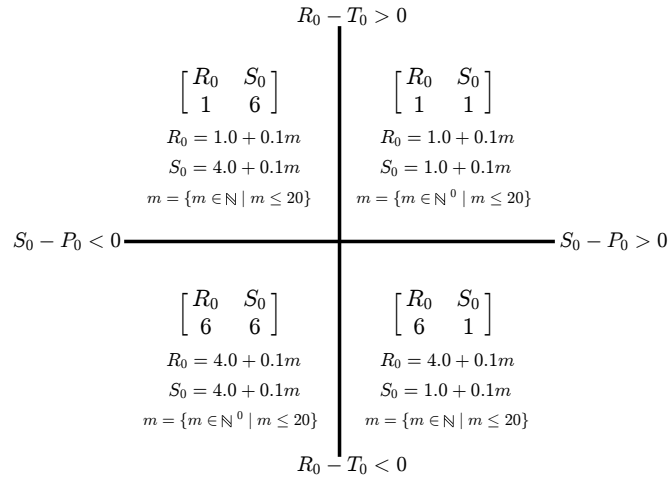
## C. Simulation parameters

We choose  $\Delta x = 1$  and  $\Delta t = 0.05$  to ensure the stability of 2D diffusion algorithm. Stability is ensured when  $D_n \frac{\Delta t}{\Delta x^2} \leq \frac{1}{4}$  [S1]. We use periodic boundary conditions for spatial simulations. The scaling value  $\epsilon = 0.5$  was further chosen so that  $\Delta \tau = \Delta t / \epsilon = 0.1$ . This assures the largest transition probability of a birth-death process  $k_i \Delta \tau$  will be no larger than 1 given the values of payoff matrix chosen in all the simulations. The model parameters are in arbitrary simulation units, and the values other than  $A_0$  are shown in Table S1.

The parameters of simulations in FIG. 1 are shown in Table S1 and FIG. S1. In FIG. 1, each plot for stochastic individual-based model dynamics are averaged over 100 replicates except for oscillatory dynamics, given phase differences that can arise due to demographic noise. The parameters except for  $D_n$  of simulations in FIG. 2 are shown in Table S1 and FIG. S2.  $D_n$  is specified on each panel of FIG. 2 in the main text. The axes of heat maps ranging from -2 to 2, linearly increase with difference 0.1 on both the horizontal axis,  $S_0 - P_0$  and the vertical axis,  $R_0 - T_0$ . There are thus  $41 \cdot 41 = 1681$  grids on each heat map. The value of each grid on the heat maps is the average over 20 replicates, so there are information of  $41 \cdot 41 \cdot 20 \cdot 4 = 134480$  simulations in FIG. 2. The parameters except for  $D_n$  of simulations in FIG. 3 are shown in Table S1 and  $A_0 = \begin{bmatrix} 2.5 & 5.5 \\ 1 & 6 \end{bmatrix}$ .  $D_n$  is specified on each panel of FIG. 3 in the main text.

TABLE S1: Model parameter values in simulation units.

Variable	Value
$A_1$	$\begin{bmatrix} 3 & 0 \\ 5 & 1 \end{bmatrix}$
$A_0$	see below for each figure
$N$	10000
$\epsilon$	0.5
$\theta$	2
$D_n$	$[0, 1, \infty]$
$L$	100
$(x_0, n_0)$	(0.3, 0.7)

FIG. S1: The values of matrix  $A_0 = \begin{bmatrix} R_0 & S_0 \\ T_0 & P_0 \end{bmatrix}$  in each section on the parameter space of FIG. 1 in the main text.FIG. S2: The values of matrix  $A_0 = \begin{bmatrix} R_0 & S_0 \\ T_0 & P_0 \end{bmatrix}$  in each section on the parameter space of FIG. 2 in the main text.

#### D. Classification Criteria for TOC and averted dynamics

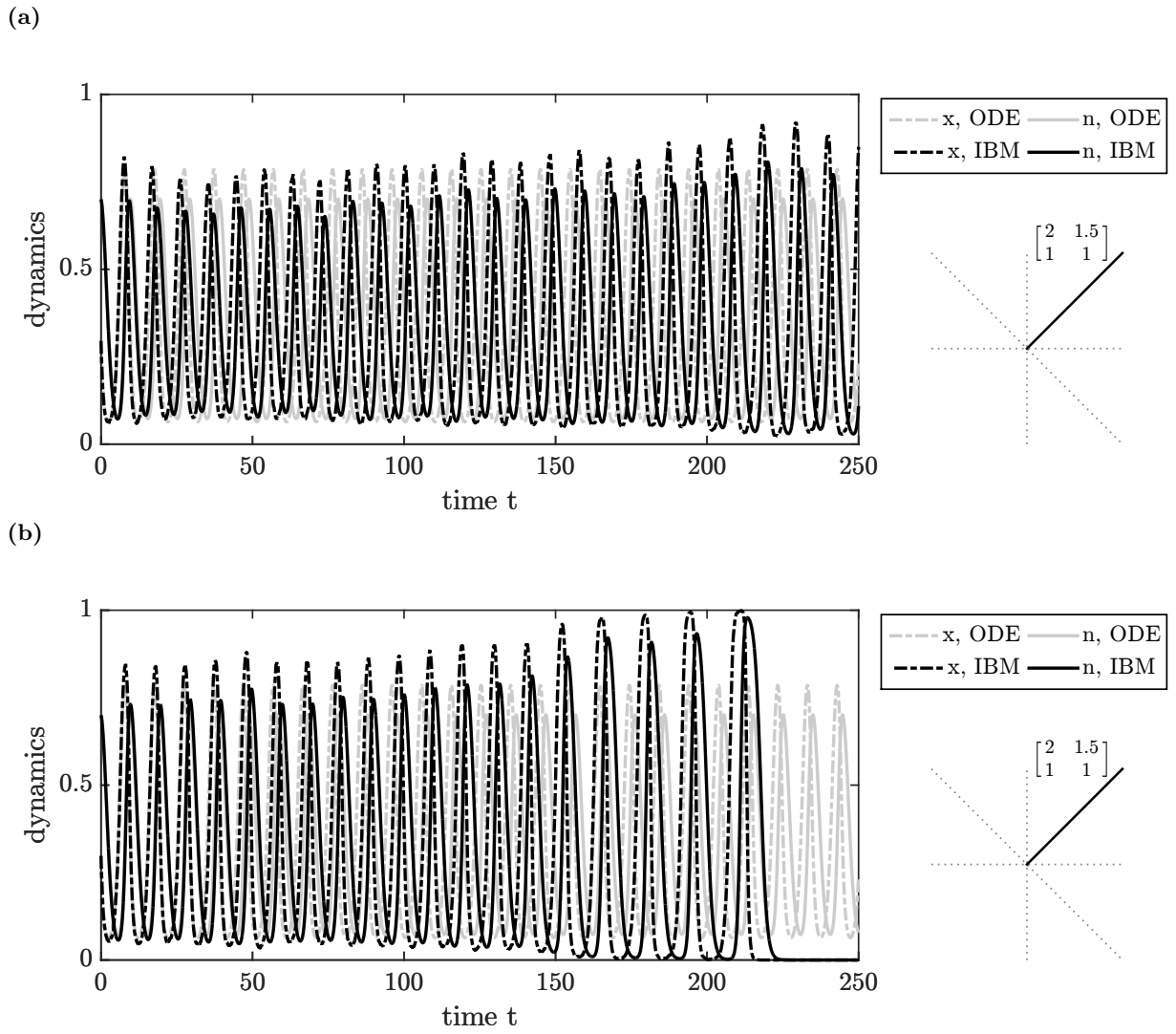
The classification criteria for characterizing temporal dynamics beyond the transient phase of dynamics into TOC or non-TOC is as follows:

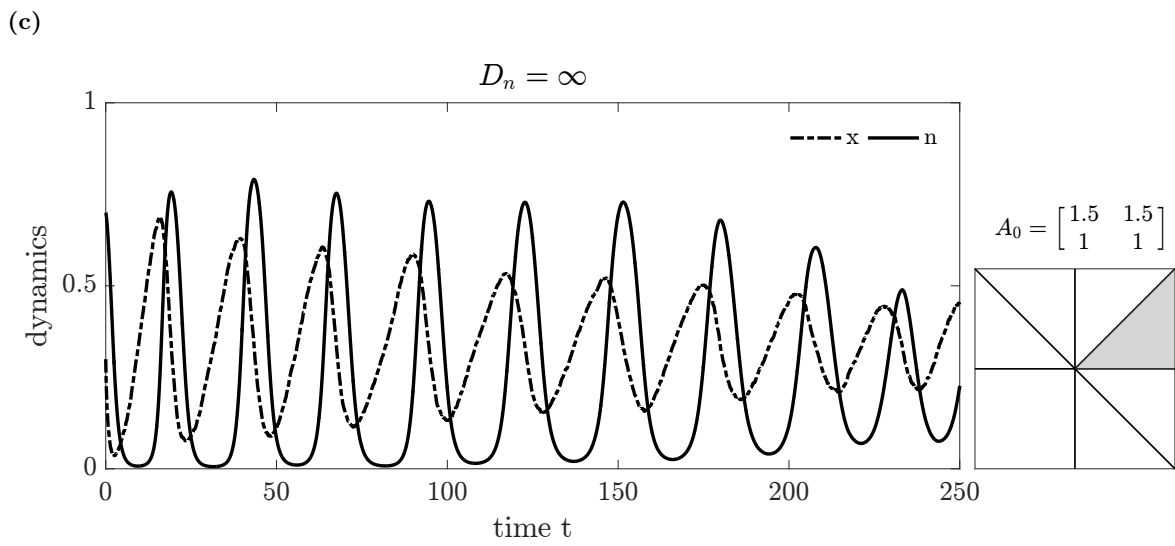
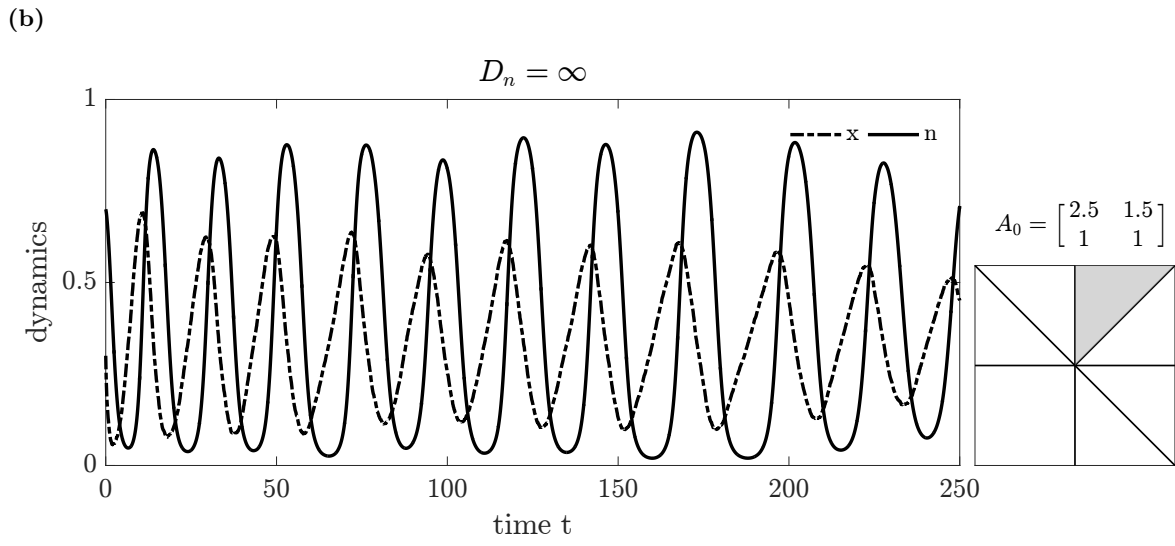
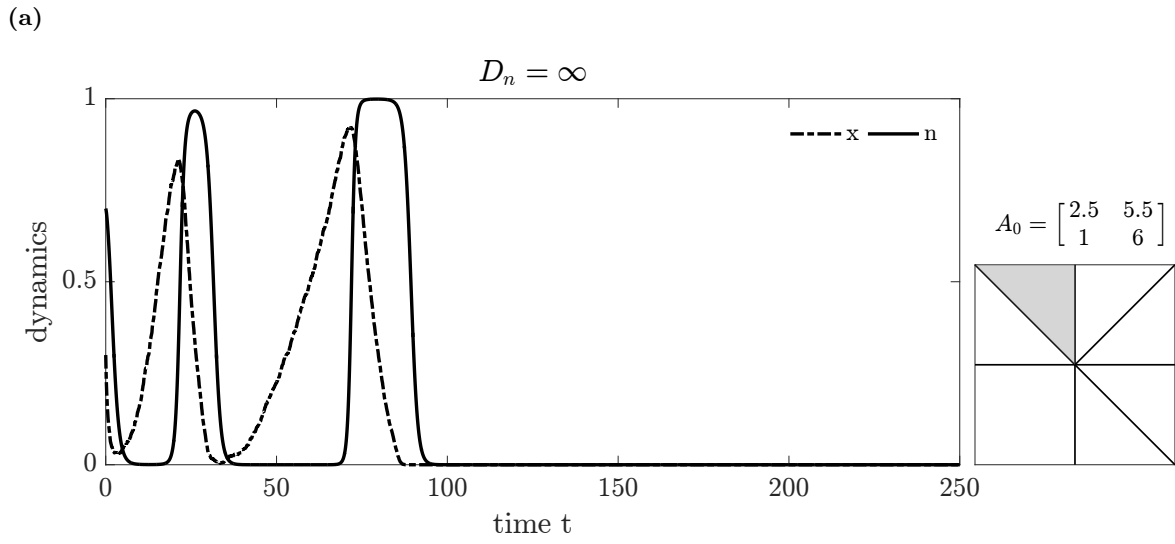
- Find the difference between consecutive peaks and valleys in the environment,  $\delta n$ , and in the fraction of cooperators,  $\delta x$ .
  - if the maximum  $\delta n$  or  $\delta x$  is larger than the threshold  $1 - 2\delta$ , it indicates the dynamics is an oscillating TOC because of the large variation in magnitude.  $\delta$  is a smaller number set to be 0.01.
  - else, we take the mean of the later 20% time series of  $x(t)$  and  $n(t)$ , i.e.,  $\bar{x}$  and  $\bar{n}$  respectively. The classification into a TOC is as follows:
    - \* if  $\bar{n} < \delta$ , it is a TOC.
    - \* else, a TOC is averted.

To separate quasi-periodic dynamics from an oscillating TOC, we categorize a dynamics as an o-TOC if the amplitude is large enough (maximum  $\delta n > 1 - 2\delta$  or  $\delta x > 1 - 2\delta$ ). This decision stump allows us to classify dynamics with small to moderate oscillations as averted. After separating o-TOC from other oscillating dynamics, a trajectory is classified as a TOC if the environment is drained at the later part of the simulation, namely  $\bar{n} < \delta$  regardless what the value of  $\bar{x}$  is.

### III. SPATIAL-TEMPORAL DYNAMICS SIMULATION RESULTS

FIG. S3 shows how demographic noise in non-spatial individual based models (IBM) can change the system dynamics. The analysis of the ODE system (Eq. 2 and Eq. 3 in the main text) predicts neutral orbits when  $(R_0 - T_0)/(S_0 - P_0) = \theta$  (gray lines) [S2], but the non-spatial IBM simulations reveal that the perfect orbits are impossible due to stochasticity. We can see in FIG. S3 that demographic noise modulates the amplitudes of oscillations substantially. The increased amplitudes can drive the system toward a boundary and may even lead to a TOC (FIG. S3(b)). Oscillations may also be induced by strong coupling between local sites mediated by diffusing environment. As shown in FIG. S4, oscillations are present across a large range of the  $(S_0 - P_0) - (R_0 - T_0)$  parameter space. Some of the oscillations may lead to a TOC (FIG. S4(a)), while others may have various amplitudes but the population persists over multiple runs, in these cases until the end of the simulation (FIG. S4(b) - FIG. S4(d)). Given the absorbing conditions of the stochastic model, we cannot guarantee infinite-time persistence of oscillations in any finite simulation.





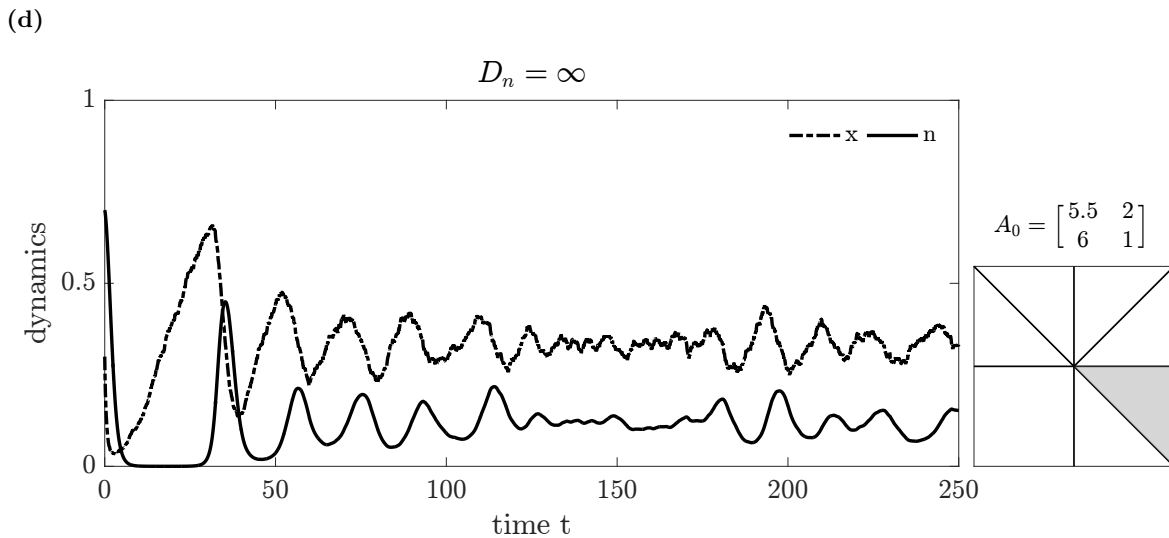


FIG. S4: The oscillating dynamics are common with  $D_n = \infty$  in a wide range of  $A_0$ . These four plots shows the temporal dynamics of a replicate with a specific  $A_0$ , and where it falls on the  $(S_0 - P_0) - (R_0 - T_0)$  parameter space in the each inserted plot. The values of  $A_0$ 's are (a)  $\begin{bmatrix} 2.5 & 5.5 \\ 1 & 6 \end{bmatrix}$ , (b)  $\begin{bmatrix} 2.5 & 1.5 \\ 1 & 1 \end{bmatrix}$ , (c)  $\begin{bmatrix} 1.5 & 1.5 \\ 1 & 1 \end{bmatrix}$ , and (d)  $\begin{bmatrix} 5.5 & 2 \\ 6 & 1 \end{bmatrix}$ , respectively.

- 
- [S1] W. H. Press, S. A. Teukolsky, W. T. Vetterling, and B. P. Flannery, *Numerical Recipes 3rd Edition: The Art of Scientific Computing* (Cambridge University Press, 2007) Chap. 20.
- [S2] J. S. Weitz, C. Eksin, K. Paarporn, S. P. Brown, and W. C. Ratcliff, *Proceedings of the National Academy of Sciences* **113**, E7518 (2016).